Could two NMSSM Higgs bosons be present near 125 GeV?

John F. Gunion, Yun Jiang, and Sabine Kraml

Could two NMSSM Higgs bosons be present near 125 GeV?

John F. Gunion[*] and Yun Jiang[†]

Department of Physics, University of California, Davis, CA 95616, USA

Sabine Kraml[‡]

*Laboratoire de Physique Subatomique et de Cosmologie, UJF Grenoble 1,
CNRS/IN2P3, INPG, 53 Avenue des Martyrs, F-38026 Grenoble, France*

We examine GUT-scale NMSSM scenarios in which *both* h_1 and h_2 lie in the 123–128 GeV mass range. Very substantially enhanced $\gamma\gamma$ and other rates are possible. Broadened mass peaks are natural.

Keywords: Supersymmetry phenomenology, Higgs physics

Data from the ATLAS and CMS collaborations [1–3] provide an essentially 5σ signal for a Higgs-like resonance with mass of order 123–128 GeV. In the $\gamma\gamma$ final state, the ATLAS and CMS rates are roughly 1.9 ± 0.4 and 1.6 ± 0.4 times the Standard Model (SM) prediction. In the $ZZ \to 4\ell$ channel, the ATLAS and CMS signals are roughly $1.1^{+0.5}_{-0.4}$ and $0.7^{+0.4}_{-0.3}$ times the SM expectation, respectively. In the $b\bar{b}$, $\tau^+\tau^-$ and $WW \to \ell\nu\ell\nu$ channels, the central value ATLAS rates are somewhat suppressed relative to the SM prediction but error bars are very large. The CMS signals in these latter channels are also somewhat suppressed and lie at least 1σ below the SM prediction — no signal being observed in the $\tau^+\tau^-$ channel. Meanwhile, the CDF and D0 experiments have announced new results [4] that support the ~ 125 GeV Higgs signal and suggest an enhancement relative to the SM of the W+Higgs with Higgs$\to b\bar{b}$ rate by a factor of 2 ± 0.6.

Enhanced rates in the $\gamma\gamma$ channel have been shown to be difficult to achieve in the NMSSM [5], while remaining consistent with all relevant constraints, including those from LEP searches, B-physics, the muon anomalous magnetic moment, $a_\mu \equiv (g-2)_\mu/2$, and the relic density of dark matter, Ωh^2, when parameters are semi-unified at the GUT scale. By "semi-unified" we mean a model in which m_0, $m_{1/2}$, and A_0 are universal at the GUT scale with NUHM relaxation for $m^2_{H_u}$, $m^2_{H_d}$ and m^2_S and general A_λ and A_κ. Enhancements appear to be possible only if large values of the superpotential coupling λ are employed and the a_μ constraint is greatly relaxed [6]. (See [7] for the first discussion of an enhanced $\gamma\gamma$ rate at large λ in the NMSSM with parameters defined at the weak scale.) In this case an enhancement arises when the h_1 and h_2 are sufficiently close in mass that one Higgs, h_i, "steals" (through mixing) some of the $b\bar{b}$ width of the other Higgs, h_j. When this happens it is generically the case that the gg and $\gamma\gamma$ partial widths of the h_j are much less affected and so $BR(h_j \to \gamma\gamma)$ is significantly enhanced, $b\bar{b}$ being the dominant contribution to the total width. In this Letter, we pursue the case of generally large λ and uncover a particularly interesting set of scenarios in which the two lightest CP-even Higgs bosons, h_1 and h_2, both lie in the 123–128 GeV mass window. In this case, a second mechanism for large $\gamma\gamma$ rates emerges — namely both h_1 and h_2 contribute significantly and their summed rate is enhanced even though their individual rates are more or less at, or even somewhat below, the SM level. Phenomenological consequences of these degenerate scenarios are examined. Enhanced $\gamma\gamma$ signals in the NMSSM context have also been considered in [8–10], the latter two noting the possible importance of light stau loop or light chargino loop, respectively, contributions to the $\gamma\gamma$ coupling of a ~ 126 GeV Higgs boson. In our semi-unified GUT scale parameter approach, these are never significant.

For the numerical analysis, we use NMSSMTools [11][12][13] version 3.2.0, which has improved convergence of RGEs in the case of large Yukawa couplings and thus allows us to explore parameter regions that were left uncharted in [5]. The precise constraints imposed are the following. Our 'basic constraints' will be to require that an NMSSM parameter choice be such as to give a proper RGE solution, have no Landau pole, have a neutralino as the lightest SUSY particle (LSP) and obey Higgs and SUSY mass limits as implemented in NMSSMTools-3.2.0.[1]

Regarding B physics, the constraints considered are those on $\text{BR}(B_s \to X_s\gamma)$, ΔM_s, ΔM_d, $\text{BR}(B_s \to \mu^+\mu^-)$, $\text{BR}(B^+ \to \tau^+\nu_\tau)$ and $\text{BR}(B \to X_s\mu^+\mu^-)$ at 2σ as encoded in NMSSMTools-3.2.0, except that we updated the bounds on rare B decays to $3.04 < \text{BR}(B_s \to X_s\gamma) \times 10^4 < 4.06$ and $\text{BR}(B \to \mu^+\mu^-) < 4.5 \times 10^{-9}$; theoretical uncertainties in B-physics observables are taken into account as implemented in NMSSMTools-3.2.0.

Regarding dark matter constraints, we accept all points that have $\Omega h^2 < 0.136$, thus allowing for scenarios in which the relic density arises at least in part from some other source. However, we single out points with $0.094 \leq \Omega h^2 \leq 0.136$,

---

[*] jfgunion@ucdavis.edu

[†] yunjiang@ucdavis.edu

[‡] sabine.kraml@lpsc.in2p3.fr

[1] Higgs mass limits are from LEP, TEVATRON, and early LHC data; SUSY mass limits are essentially from LEP. As we will see, the gluino and squark masses that result from imposing the 'basic constraints' and requiring a Higgs signal consistent with observations are so high that current LHC data do not imply further constraints on SUSY masses.

which is the 'WMAP window' defined in NMSSMTools-3.2.0 after including theoretical and experimental systematic uncertainties. In addition, we impose bounds on the spin-independent LSP–proton scattering cross section implied by the neutralino-mass-dependent Xenon100 bound [14]. (For points with $\Omega h^2 < 0.094$, we rescale these bounds by a factor of $0.11/\Omega h^2$.)

Our study focuses in particular on NMSSM parameter choices such that both m_{h_1} and m_{h_2} lie within 123–128 GeV. We focus moreover on $\lambda \geq 0.1$, a range for which it is known [6][7] that some enhancement, relative to the SM, of the Higgs signal in the $\gamma\gamma$ final state is possible. The degenerate situation is especially interesting in that an enhanced $\gamma\gamma$ rate at ~ 125 GeV could arise as a result of the h_1 and h_2 rates summing together, even if the individual rates are not full SM-like strength (or enhanced).

Above, we did not mention imposing a constraint on a_μ. In fact, given the previously defined constraints and focusing on $\lambda \geq 0.1$, δa_μ is always too small, being at most $\sim 2 \times 10^{-10}$, while the desired range would be $5.77 \times 10^{-10} < \delta a_\mu < 4.91 \times 10^{-9}$ (including a theoretical uncertainty of $\pm 3 \times 10^{-10}$). Demanding δa_μ large enough to fall into the above window, or even come close to doing so, appears from our scans to date to only be possible if $\lambda < 0.1$ [5], for which the Higgs signal in the $\gamma\gamma$ and VV^* ($V = W, Z$) final states for Higgs in the 123–128 GeV window is very SM-like. In this work we neglect the a_μ constraint from now on, and we are therefore implicitly assuming that the observed discrepancy in a_μ comes, at least in part, from a source other than the NMSSM.

The main production/decay channels relevant for current LHC data are gluon-gluon and WW fusion to Higgs with Higgs decay to $\gamma\gamma$ or $ZZ^* \to 4\ell$. The LHC is also beginning to probe W, Z+Higgs with Higgs decay to $b\bar{b}$, a channel for which Tevatron data is relevant, and $WW \to$Higgs with Higgs$\to \tau^+\tau^-$. For the cases studied, where there are two nearly degenerate Higgs bosons, we will combine their signals as follows in defining the mass and signal for the effective Higgs, h. First, for the individual Higgs we compute the ratio of the $Y = gg$ or WW-fusion (Y=VBF) induced Higgs cross section times the Higgs branching ratio to a given final state, X, relative to the corresponding value for the SM Higgs boson: $R_Y^{h_i}(X) \equiv \frac{\Gamma(h_i \to Y)\; \mathrm{BR}(h_i \to X)}{\Gamma(h_{\mathrm{SM}} \to Y)\; \mathrm{BR}(h_{\mathrm{SM}} \to X)}$, where h_i is the ith NMSSM scalar Higgs, and h_{SM} is the SM Higgs boson; see [5] for details. Note that the corresponding ratio for $V^* \to Vh_i$ ($V = W, Z$) with $h_i \to X$ is equal to $R_{\mathrm{VBF}}^{h_i}(X)$. These ratios are computed in a self-consistent manner (that is, treating radiative corrections for the SM Higgs boson in the same manner as for the NMSSM Higgs bosons) using an appropriate additional routine for the SM Higgs added to the NMHDECAY component of the NMSSMTools package. Next, we compute the effective Higgs mass in given production and final decay channels Y and X, respectively, as $m_h^Y(X) \equiv \frac{R_Y^{h_1}(X)m_{h_1} + R_Y^{h_2}(X)m_{h_2}}{R_Y^{h_1}(X) + R_Y^{h_2}(X)}$ and define the net signal to simply be $R_Y^h(X) = R_Y^{h_1}(X) + R_Y^{h_2}(X)$. Of course, the extent to which it is appropriate to combine the rates from the h_1 and h_2 depends upon the degree of degeneracy and the experimental resolution. For the latter, we assume $\sigma_{\mathrm{res}} \sim 1.5$ GeV [15].[2] It should be noted that the widths of the h_1 and h_2 are of the same order of magnitude as the width of a 125 GeV SM Higgs boson, $i.e.$ they are very much smaller than this resolution.

We perform scans covering the following parameter ranges, which correspond to an expanded version of those considered in [6]: $0 \leq m_0 \leq 3000$; $100 \leq m_{1/2} \leq 3000$; $1 \leq \tan\beta \leq 40$; $-6000 \leq A_0 \leq 6000$; $0.1 \leq \lambda \leq 0.7$; $0.05 \leq \kappa \leq 0.5$; $-1000 \leq A_\lambda \leq 1000$; $-1000 \leq A_\kappa \leq 1000$; $100 \leq \mu_{\mathrm{eff}} \leq 500$. In the figures shown in the following, we only display points which pass the basic constraints, satisfy B-physics constraints, have $\Omega h^2 < 0.136$, obey the XENON100 limit on the LSP scattering cross-section off protons *and* have *both* h_1 and h_2 in the desired mass range: 123 GeV $< m_{h_1}, m_{h_2} < 128$ GeV.

In Fig. 1, we display $R_{gg}^{h_2}(\gamma\gamma)$ versus $R_{gg}^{h_1}(\gamma\gamma)$ with points color coded according to $m_{h_2} - m_{h_1}$. The circular points have $\Omega h^2 < 0.094$, while diamond points have $0.094 \leq \Omega h^2 \leq 0.136$ ($i.e.$ within the WMAP window). We observe a large number of points for which $m_{h_1}, m_{h_2} \in [123, 128]$ GeV and many are such that $R_{gg}^{h_1}(\gamma\gamma) + R_{gg}^{h_2}(\gamma\gamma) > 1$. A few such points have Ωh^2 in the WMAP window. However, the majority of the points with $R_{gg}^{h_1}(\gamma\gamma) + R_{gg}^{h_2}(\gamma\gamma) > 1$ have Ωh^2 below the WMAP window and for many the $\gamma\gamma$ signal is shared between the h_1 and the h_2.

Based on these results, we will now combine the h_1 and h_2 signals as described above and present plots coded according to the following legend. First, we note that circular (diamond) points have $\Omega h^2 < 0.094$ ($0.094 \leq \Omega h^2 \leq 0.136$). We then color the points according to: red for $m_{h_2} - m_{h_1} \leq 1$ GeV; blue for 1 GeV $< m_{h_2} - m_{h_1} \leq 2$ GeV; green for 2 GeV $< m_{h_2} - m_{h_1} \leq 3$ GeV. For current statistics and $\sigma_{\mathrm{res}} \gtrsim 1.5$ GeV we estimate that the h_1 and h_2 signals will not be seen separately for $m_{h_2} - m_{h_1} \leq 2$ GeV.

In the first three plots of Fig. 2 we show results for $R_{gg}^h(X)$ with $m_h^{gg}(X) \in [123, 128]$ GeV, where $m_h^{gg}(X)$ was defined above, for $X = \gamma\gamma, VV, b\bar{b}$. Enhanced $\gamma\gamma$ and VV rates from gluon fusion are very common. We note that there is a very strong correlation between $R_{gg}^h(\gamma\gamma)$ and $R_{gg}^h(VV)$ described approximately by $R_{gg}^h(\gamma\gamma) \sim 1.25\, R_{gg}^h(VV)$. In particular, if $R_{gg}^h(\gamma\gamma) \sim 1.5$, as suggested by current experimental results, then in this model $R_{gg}^h(VV) \geq 1.2$. Given

---

[2] The values for σ_{res} quoted in this paper range from 1.39–1.84 GeV to 2.76–3.19 GeV, the better resolutions being for the case where both photons are in the barrel and the worse resolutions for when one or both photons are in the endcap. We anticipate that the more recent analyses have achieved substantially better mass resolutions, but details are not yet available.
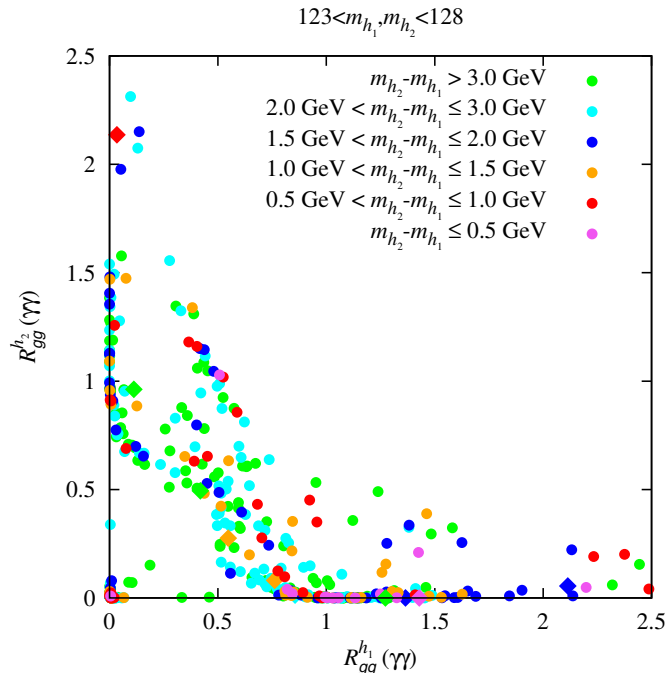
FIG. 1. Correlation of $gg \to (h_1, h_2) \to \gamma\gamma$ signal strengths when both h_1 and h_2 lie in the 123–128 GeV mass range. The circular points have $\Omega h^2 < 0.094$, while diamond points have $0.094 \leq \Omega h^2 \leq 0.136$. Points are color coded according to $m_{h_2} - m_{h_1}$ as indicated on the figure.

this correlation, it is not surprising that the m_h values for the gluon fusion induced $\gamma\gamma$ and VV final states are also strongly correlated — in fact, they differ by no more than a fraction of a GeV and are most often much closer. The bottom-right plot of Fig. 2 shows that enhancement of Wh production with $h \to b\bar{b}$ is rather limited; indeed the maximal value of $R^h_{\mathrm{VBF}}(b\bar{b}) = R^h_{W^* \to Wh}(b\bar{b})$ is of order 1.2, a value that falls short of the best fit value suggested by the new Tevatron analysis [4].

The primary mechanism behind the enhanced $\gamma\gamma$ rate is that large net $\gamma\gamma$ branching ratio is achieved by reducing the average total width by reducing the average $b\bar{b}$ coupling strength. This leads to the aniti-correlation between $R^h_{gg}(\gamma\gamma)$ and $R^h_{W^* \to Wh}(b\bar{b}) = R^h_{\mathrm{VBF}}(b\bar{b})$ noted just above. In general, the larger $R^h_{gg}(\gamma\gamma)$ is, the smaller the value of $R^h_{W^* \to Wh}(b\bar{b})$. However, we do observe that there *are* parameter choices for which both the $\gamma\gamma$ rate at the LHC and the $W^* \to Wh(\to b\bar{b})$ rate at the Tevatron (and LHC) can be enhanced relative to the SM as a result of there being contributions to these rates from both the h_1 and h_2. It is often the case that one of the h_1 or h_2 dominates $R^h_{gg}(\gamma\gamma)$ while the other dominates $R^h_{W^* \to Wh}(b\bar{b})$. However, a significant number of the points are such that either the $\gamma\gamma$ or the $b\bar{b}$ signal receives substantial contributions from both the h_1 and the h_2 (as seen, for example, in Fig. 1 for the $\gamma\gamma$ final state) while the other final state is dominated by just one of the two Higgses. We did not find points where the $\gamma\gamma$ and $b\bar{b}$ final states *both* receive substantial contributions from *both* the h_1 and h_2.

We can summarize the dependence of $R^h_{gg}(\gamma\gamma)$ on λ, κ, $\tan\beta$ and μ_{eff} as follows. $R^h_{gg}(\gamma\gamma) > 1.2, 1.5, 2.0$ for $\lambda \in [0.33, 0.68], [0.4, 0.68], [0.58, 0.68]$, $\kappa \in [0.15, 0.44], [0.21, 0.4], [0.29, 0.4]$, $\tan\beta \in [2, 14]], [2, 14], [2, 4.2]$ and $\mu_{\mathrm{eff}} \in [107, 260], [110, 180], [110, 127]$ GeV, respectively. Such low values of μ_{eff} are very favorable in point of view of fine tuning, in particular if stops are also light. Indeed a good fraction of our points with degenerate h_1, h_2 and $R(\gamma\gamma) > 1$ features light stops with $m_{\tilde{t}_1} \in [300, 700]$ GeV and $M_{\mathrm{SUSY}} = \sqrt{m_{\tilde{t}_1} m_{\tilde{t}_2}} \lesssim 1$ TeV. The stop mixing is typically, but not necessarily, large in these cases, $(A_t - \mu_{\mathrm{eff}} \cot\beta)/M_{\mathrm{SUSY}} \approx 1.5$–2.

Implications of the enhanced $\gamma\gamma$ rate scenarios for other particles are also quite interesting. First, in Fig. 3 we plot all points without any cut on $R^h_{gg}(\gamma\gamma)$. We see that our scenarios have squark and gluino masses that are above about 1.25 TeV ranging up to as high as 6 TeV (where our scanning more or less ended). This result continues to apply even if we impose a cut of $R^h_{gg}(\gamma\gamma) > 1.3$. There is also significant correlation between the possible values of $R^h_{gg}(\gamma\gamma)$ and the masses of the other Higgs bosons. Noting that $m_{a_2} \simeq m_{h_3} \simeq m_{H^\pm}$, we can summarize in terms of m_{a_1} and $m_{H^\pm}$. The general trend is that the maximum $R^h_{gg}(\gamma\gamma)$ possible decreases rapidly as m_{a_1} and $m_{H^\pm}$ increase. In more detail, values of $R^h_{gg}(\gamma\gamma) > 2.3, 1.5, 1$ are associated with $m_{H^\pm} \in [270, 450], [270, 1625], [270, 2850]$ GeV and
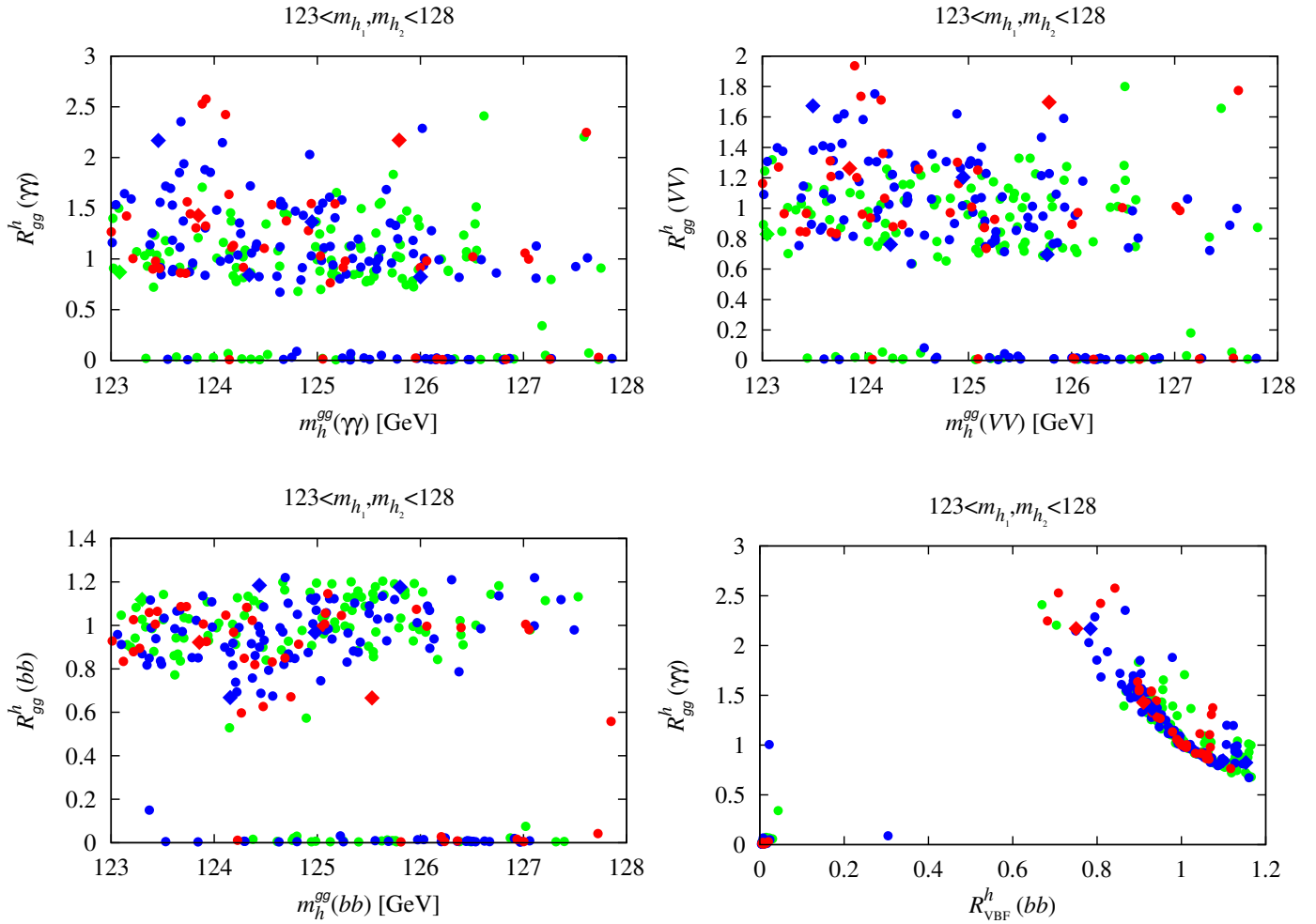
FIG. 2. The first 3 plots show $R^h_{gg}(X)$ for $X = \gamma\gamma, VV, b\bar{b}$ versus the appropriate effective Higgs mass m_h as defined in text. The final plot gives $R^h_{gg}(\gamma\gamma)$ vs. $R^h_{W^*\to Wh}(b\bar{b}) = R^h_{\rm VBF}(b\bar{b})$. The color code here and in the following figures is: green for points with $2 \text{ GeV} < m_{h_2} - m_{h_1} \le 3 \text{ GeV}$, blue for $1 \text{ GeV} < m_{h_2} - m_{h_1} \le 2 \text{ GeV}$, and red for $m_{h_2} - m_{h_1} \le 1 \text{ GeV}$.

$m_{a_1} \in [80, 130], [64, 225], [60, 730]$ GeV, respectively, 250 GeV being the lowest allowed $m_{H^\pm}$. The lowest allowed m_{a_1} with any significant $R^h_{gg}(\gamma\gamma)$ is ~ 60 GeV. While the m_{a_1} and $m_{H^\pm} \simeq m_{a_2} \simeq m_{h_3}$ masses associated with high $R^h_{gg}(\gamma\gamma)$ values are modest in size, detectability of these states at such masses requires further study. One interesting point is that although $m_{a_1} \sim 125$ GeV is common for points with $R^h_{gg}(\gamma\gamma) > 1$, the contribution of the a_1 to the $\gamma\gamma$ signal is always small, typically $R^{a_1}_{gg}(\gamma\gamma) \lesssim 0.01$ (due to the fact that the a_1 is always largely singlet for these and, indeed, all $R^h_{gg}(\gamma\gamma) > 1$ points).

Let us now focus on properties of the LSP. In the plots of Fig. 4, we display Ωh^2 and the spin-independent cross section for LSP scattering on protons, $\sigma_{\rm SI}$, for the points plotted in previous figures. A large fraction of the points have small $\mu_{\rm eff}$, in which case the LSP is dominantly higgsino implying that Ωh^2 will be too low.

Regarding the GUT-scale parameters associated with the points plotted in previous figures, we note that points with $R^h_{gg}(\gamma\gamma) > 1.3$ have $m_0 \in [0.65, 3]$ TeV, $m_{1/2} \in [0.5, 3]$ TeV, $A_0 \in [-4.2, -0.8]$ TeV, $A_\kappa \in [-500, +450]$ GeV, $A_\lambda \in [-750, +550]$ GeV, $m_S(\text{GUT}) \in [1.2, 4.2]$ TeV, $m_{H_u}(\text{GUT}) \in [1.7, 17]$ TeV, $m_{H_d}(\text{GUT}) \in [\sim 0, 4.2]$ TeV, $\lambda \in [0.33, 0.67]$, $\kappa \in [0.22, 0.36]$, and $\tan\beta \in [2, 14]$.

We have already noted that it is not possible to find scenarios of this degenerate/enhanced type while predicting a value of δa_μ consistent with that needed to explain the current discrepancy. In particular, the very largest value of δa_μ achieved is of order 1.8×10^{-10}.

Finally, we mention some properties of the (diamond) points with Ωh^2 in the WMAP window. Of course, since such points comprise only 1.6% of the total sample, it is very possible that they do not cover the full WMAP region and it is
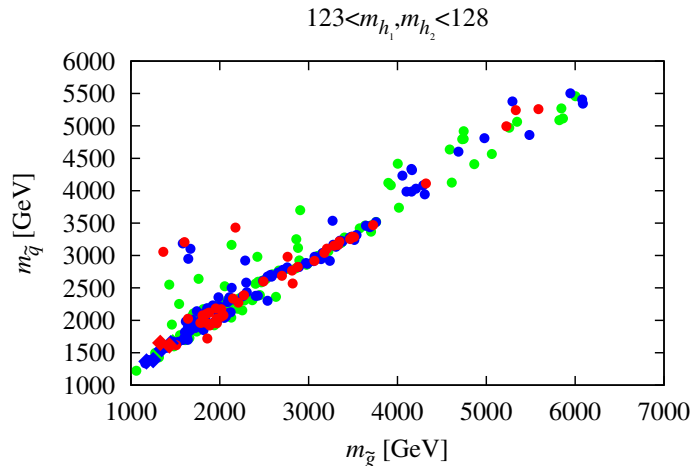
FIG. 3. Average light-flavor squark mass, $m_{\tilde{q}}$, versus gluino mass, $m_{\tilde{g}}$, for the points plotted in the previous figures.

thus hard to be certain as to how well they exemplify the properties of a larger sample of such points. First, about half of our WMAP-window points show enhanced rates, and for two of these points either $R^{h_1}_{gg}(\gamma\gamma) > 2$ or $R^{h_2}_{gg}(\gamma\gamma) > 2$, with the R for the other Higgs being small. The WMAP-window points with large $R^h_{gg}(\gamma\gamma)$ are located at low masses of $m_{\tilde{g}} \sim 1.3$ TeV and $m_{\tilde{q}} \sim 1.6$ TeV. Moreover, all points in the WMAP window have $m_{\tilde{t}_1} \in [300, 700]$ GeV. Also, WMAP-window points have a rather limited range of LSP masses, roughly $m_{\tilde{\chi}^0_1} \in [60, 80]$ GeV. They have large enough Ωh^2 since they are mixed higgsino–singlino, with a singlino component of the order of 20%, see the bottom-row plots of Fig. 4. Finally, the WMAP-window points with large $R^h_{gg}(\gamma\gamma, VV)$ have $\delta a_\mu < 6 \times 10^{-11}$.

To summarize, we have identified a set of interesting NMSSM scenarios in which the two lightest CP-even Higgs bosons are closely degenerate and lie in the 123–128 GeV mass window. Large rates (relative to $gg \to h_{\rm SM} \to \gamma\gamma$ or $gg \to h_{\rm SM} \to ZZ^* \to 4\ell$) for $gg \to h_{1,2} \to \gamma\gamma$ and $gg \to h_{1,2} \to ZZ^* \to 4\ell$ are possible, sometimes because one of the rates is large but also sometimes because the rates are comparable and their sum is large. This suggests that, especially if enhanced rates continue to be observed in these channels, it will be important for the experimental community to be on the lookout for mass peaks in $m_{\gamma\gamma}$ and $m_{4\ell}$ that are broader than expected purely on the basis of the experimental mass resolution. In addition, the apparent mass in the $\gamma\gamma$ final state might differ slightly from the apparent mass in the 4ℓ final state. Significant statistics will be required to resolve such features.
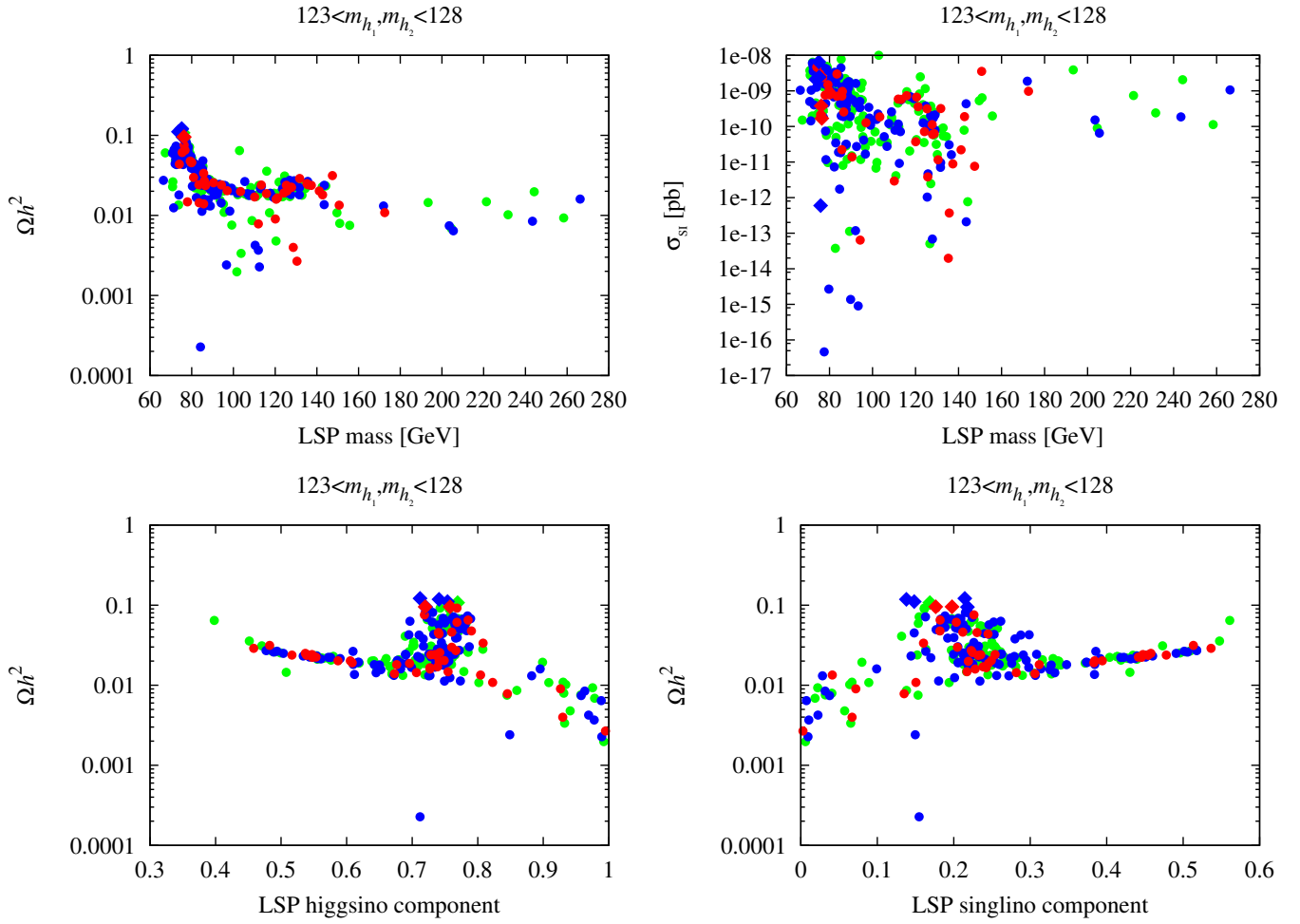
ACKNOWLEDGMENTS

FIG. 4. Top row: Ωh^2 and spin-independent cross section on protons versus LSP mass for the points plotted in previous figures. Bottom row: Ωh^2 versus LSP higgsino (left) and singlino (right) components.

[1] J. Incandela, F. Gianotti, "Latest update in the search for the Higgs boson", CERN seminar on 4 July 2012, `http://indico.cern.ch/conferenceDisplay.py?confId=197461`.

[2] `http://www.atlas.ch/news/2012/latest-results-from-higgs-search.html`.

[3] `http://cms.web.cern.ch/news/observation-new-particle-mass-125-gev`.

[4] [TEVNPH Working Group], Updated Combination of CDF and D0 Searches for Standard Model Higgs Boson Production with up to 10 fb^{-1} of Data, see `http://www.fnal.gov/pub/presspass/press_releases/2012/Higgs-Tevatron-20120702.html`.

[5] J. F. Gunion, Y. Jiang and S. Kraml, The Constrained NMSSM and Higgs near 125 GeV, Phys. Lett. B **710**, 454 (2012), `arXiv:1201.0982[hep-ph]`.

[6] U. Ellwanger and C. Hugonie, Higgs bosons near 125 GeV in the NMSSM with constraints at the GUT scale, `arXiv:1203.5048[hep-ph]`.

[7] U. Ellwanger, A Higgs boson near 125 GeV with enhanced di-photon signal in the NMSSM, JHEP **1203** (2012) 044, `arXiv:1112.3548[hep-ph]`.

[8] D. A. Vasquez, G. Belanger, C. Boehm, J. Da Silva, P. Richardson and C. Wymant, arXiv:1203.3446 [hep-ph].

[9] J. -J. Cao, Z. -X. Heng, J. M. Yang, Y. -M. Zhang and J. -Y. Zhu, JHEP **1203**, 086 (2012) [arXiv:1202.5821 [hep-ph]].

[10] S. F. King, M. Muhlleitner and R. Nevzorov, Nucl. Phys. B **860**, 207 (2012) [arXiv:1201.2671 [hep-ph]].

[11] U. Ellwanger, J. F. Gunion, C. Hugonie, NMHDECAY: A Fortran code for the Higgs masses, couplings and decay widths in the NMSSM, JHEP 0502 (2005) 066, `arXiv:hep-ph/0406215`.

[12] U. Ellwanger, C. Hugonie, NMHDECAY 2.0: An Updated program for sparticle masses, Higgs masses, couplings and decay widths in the NMSSM, Comput. Phys. Commun. 175 (2006) 290–303, `arXiv:hep-ph/0508022`.

[13] `http://www.th.u-psud.fr/NMHDECAY/nmssmtools.html`.

[14] E. Aprile *et al.* [XENON100 Collaboration], Dark Matter Results from 100 Live Days of XENON100 Data, Phys. Rev. Lett. **107**, 131302 (2011), `arXiv:1104.2549[astro-ph.CO]`.

[15] S. Chatrchyan *et al.* [CMS Collaboration], Search for the standard model Higgs boson decaying into two photons in pp collisions at sqrt(s)=7 TeV, Phys. Lett. B **710**, 403 (2012), `arXiv:1202.1487[hep-ex]`.